Templated Sub-100-nm-Thick Double-Gyroid Structure from Si-Containing Block Copolymer Thin Films

Karim Aissou, Muhammad Mumtaz, Giuseppe Portale, Cyril Brochon, Eric Cloutet, Guillaume Fleury, Georges Hadziioannou

Highly-Ordered Nanoring Arrays Formed by Templated Si-Containing Triblock Terpolymer Thin Films

Karim Aissou,[1*] Muhammad Mumtaz,[1] Pierre Marcasuzaa,[1] Cyril Brochon,[1] Eric Cloutet,[1] Guillaume Fleury,[1] and Georges Hadziioannou[1]

[1]Laboratoire de Chimie des Polymères Organiques, CNRS - ENSCBP - Université de Bordeaux, B8 Allée Geoffroy Saint Hilaire, F-33615 Pessac Cedex, France

E-mail: karim.aissou@enscbp.fr

ABSTRACT: The directed self-assembly of linear triblock terpolymer chains (poly(1,1-dimethyl silacyclobutane)-*block*-polystyrene-*block*-poly(methyl methacrylate), PDMSB-*b*-PS-*b*-PMMA, noted DSM) into a thin film nanoring array is described. Self-assembly of solvent-annealed DSM thin films deposited on topographical substrates leads to highly-ordered arrays of a core/shell cylindrical structure of 38 nm period with a domain orientation controlled by the film thickness. As nanoscale arrays with vertically-oriented rings are highly desired in technological applications such as memory using magnetic recording, metamaterial, waveguide, etc., a enhanced control of the domain orientation was also demonstrated by blending DSM terpolymer chains with low molecular weight PDMSB-*b*-PS chains.

KEYWORDS: Nanoring array, thin film, self-assembly, templated substrate, solvent vapor annealing.

The production of perfectly ordered objects at the nanometer scale is attracting considerable attention due to its strong potential in creating surfaces with new functionalities. Among the panoply of nanoscale objects ordered into regular arrays, the nanoring is one of the most appealing structure to provide a significant advancement in technological applications since it exhibits unique optical,[1,2] electronic[3-6] and magnetic[7-9] properties. For instance, due its two stable vortex states consisting of clockwise or counter-clockwise circulations, the magnetic nanoring is an ideal candidate for magnetic random access memory (MRAM), since the direction of the rotating magnetic field of a ring-shaped feature can correspond to binary digital data of either “0” or “1”. Therefore, the use of ultra-dense magnetic nanoscale ring arrays has been rapidly gaining interest for next-generation MRAM, as the size and spacing of the

magnetic features can be minimized to achieve ultra-high densities without severe interaction issues encountered for either magnetic disks (for which the circular magnetization configuration can only be maintained when the disk diameter is sufficiently large) or other configurations (such as rectangles) utilizing linear magnetization mode.[10] Another key advantage of using nanoring structures is that the wavelengths of plasmon resonances can be tuned across the visible and the infrared region of the optical spectrum by simply varying the metallic ring dimensions while the electric field associated with these plasmons exhibits uniform enhancement inside the ring cavity.[11,12] These phenomena can be used to fabricate sensors based on surface enhanced Raman scattering (SERS), surface enhanced infrared absorption (SEIRA) or localized surface plasmon resonance (LSPR).

Even though ring-shaped features have considerable advantages as described above, the fabrication of highly-ordered nanoring arrays with dimensions close to the resolution limit of the conventional optical lithography is still very challenging to achieve since diffraction effects limit the proper resolution of the ring inner diameter and width.[13] Consequently the implementation of nanoring structures in advanced technological applications is restrained due to the absence of a manufacturable fabrication technique enabling large areas of ultra-high density features at low cost.

The self-assembly of linear ABC triblock terpolymer chains into a thin film core/shell cylinder structure[14] in combination with the use of topographical substrates to improve the structural long-range order[15-17] offers a powerful route to produce low-cost and highly-ordered nanoring arrays on large surfaces. Although the use of ABC block copolymer (BCP) thin films is a straightforward methodology to produce nanoring arrays on surfaces, only a few examples of out-of-plane core/shell cylinders have been reported[18-22] and none of them have demonstrated the fabrication of long-range ordered nanoscale ring arrays. To produce the metallic nanoring

arrays from the BCP templates, several approaches have been developed such as the ion bombardment of an underlying metallic surface using the BCP film as a lithographic mask[23] or the selective incorporation into BCP domains of metallic salts precursors followed by their reduction.[24] For instance, Hillmyer and coworkers reported on the fabrication of metallic nanoring arrays using PS-*b*-polydimethylsiloxane-*b*-polylactide (PS-*b*-PDMS-*b*-PLA) thin films as hard mask transfers.[22] Although they successfully demonstrated the transfer of oxidized PDMS rings into Au, $Ni_{80}Fe_{20}$ and $Ni_{80}Cr_{20}$ thin films, metallic nanorings were ordered into hexagonal arrays of ~60 nm period with limited long-range order.

In this work, we report on the directed self-assembly of Si-containing triblock terpolymer chains ordered into nanoscale ring arrays. To produce long-range ordered ring patterns, a solvent vapor annealing (SVA) methodology was used to promote the mobility of PDMSB-*b*-PS-*b*-PMMA (noted hereafter DSM) chains deposited on topographically patterned silica substrates. By using this strategy, highly-ordered core/shell cylinders with a domain orientation controlled by the film thickness were demonstrated. An effective control of the domain orientation was achieved by using a blending methodology which revealed an efficient route to fabricate templated DSM thin films with core/shell cylinders having a highly-desired out-of-plane orientation both on mesas and in trenches.

The linear DSM triblock terpolymer used in this study was prepared by a sequential anionic polymerization of (1,1-dimethyl silacyclobutane) (DMSB), styrene (S) and methyl methacrylate (MMA). To avoid side reactions with the MMA carbonyl group, a 1,1-diphenylethylene (DPE) was inserted at the end of PDMSB-*b*-PS chains before adding MMA (see **Fig. 1**). By using this methodology, PDMSB-*b*-PS-*b*-PMMA chains (Φ_{PDMSB} = 0.32, Φ_{PS} = 0.36, Φ_{PMMA} = 0.32) having a molecular weight, M_n, of 34 kg.mol^{-1} and a narrow dispersity (Đ = 1.1) were synthesized. Thin films of neat DSM or blended DSM with 25 wt. % of PDMSB-*b*-PS (noted hereafter DS) (Φ_{PDMSB} = 0.29, M_n = 21.6 kg.mol^{-1}, Đ = 1.09) were spin-coated on

templated and smooth silicon substrates using a 1 wt.% polymer solution in a mixture of tetrahydrofuran and propylene glycol monomethyl ether acetate (THF/PGMEA : 2/1). PGMEA was used to avoid the formation of periodic thickness variations (at the mm scale) on the DSM film free surface as observed on samples deposited from a pure THF solution due to the fast solvent evaporation during the spin-coating process. The film thickness, *t*, was controlled by varying the spin-coating speed (1.5-3 krpm). The self-assembly of neat and blended DSM thin films was achieved by exposing samples during different times (ranging from 1h to 3h) to a continuous stream of $CHCl_3$ vapor produced by bubbling nitrogen gas through the liquid solvent as described previously.[25] This continuous flow system was used to control the $CHCl_3$ vapor pressure in the chamber by dilution with a separate N_2 stream so that the solvent vapor consisted of 16 sccm $CHCl_3$ vapor and 4 sccm N_2 (total 20 sccm) swelled the polymer layers without dewetting. Solvent-annealed terpolymer thin films were quenched in air by quickly removing the lid of the chamber then, a CF_4/O_2 reactive ion etch (RIE) treatment was subsequently applied to preferentially remove PDMSB and PMMA domains (plasma conditions are 40 W, 17 sccm CF_4 and 3 sccm O_2) prior AFM characterization.

Figure 1a shows the structure of the DSM triblock terpolymer used in this work. This triblock terpolymer is non-frustrated[26] since the Flory-Huggins interaction parameter, χ_{DM}, between the two end-blocks (*i.e.* PDMSB and PMMA) is higher than the other pairs χ_{DS} and χ_{SM} ($\chi_{SM} \sim 0.04$[27] $< \chi_{DS} \sim 0.07$[28] $< \chi_{DM} \sim 0.2$[29] at 298K). The AFM phase image presented on **Figure 1b** shows a solvent-annealed (3h, $CHCl_3$) 27 nm thick DSM film treated by a CF_4/O_2 RIE plasma from which an out-of-plane core/shell morphology arranged into a hexagonal array with a period of ~ 38 nm can be observed. Here a fluorine-rich plasma was applied to remove the PDMSB surface wetting layer formed during the SVA process which revealed PS nanorings since the PDMSB matrix and PMMA core domains were partially etched during the plasma treatment. As apparent in **Figure 1b**, most of rings do not appear perfectly circular since BCP

domains adjust their sizes and shapes in response to the stress fields associated with the defect sites.[30,31]

As the vapor of $Al(CH_3)_3$ interacts preferentially with the carbonyl groups through metal-ligand coordination, the PMMA domains were selectively decorated by the metal precursor which serves as nucleation sites for the growth of Al_2O_3 by atomic layer deposition in a bottom-up fashion with molecular precision.[32] Therefore to confirm that PMMA is located in core domains as depicted in the inset of **Figure 1b**, the DSM thin film morphology has been infiltrated by 3 cycles of Al_2O_3 ALD followed by a UV/O_3 treatment (10 min). AFM topographic images presented on **Figure 2** show a solvent-annealed (3h, $CHCl_3$) 27 nm thick DSM film partially etched by a CF_4/O_2 RIE plasma (see **Fig. 2a**) followed by a Al_2O_3 deposition and UV/O_3 treatment (see **Fig. 2b**). It is noteworthy that PMMA domains are less apparent in AFM topographic mode than in phase contrast one (see **Fig. 1b**). Before the Al_2O_3 deposition, the solvent-annealed DSM thin film is self-assembled into a polycrystalline array of out-of-plane core/shell cylinders with a period of ~ 38 nm. In contrast, a hexagonal Al_2O_3 pattern templated from the DSM thin film is produced after the Al_2O_3 deposition process indicating the core/shell morphology consisted of a PMMA core with a PS shell surrounded by a PDMSB matrix. It is noteworthy that the Al_2O_3 dot diameter is larger than the template feature dimension which is due to the fact that the size of Al_2O_3 domains could be tuned with the number of cycles.[32]

The control of the long-range order of the core/shell morphology has been achieved by using topographical gratings in silica with a period of 500 nm consisted of 250 nm wide, 45 nm deep trenches separated by 250 nm width mesas. The AFM topographic image presented on **Figure 3a** shows a solvent-annealed (3h, $CHCl_3$) DSM thin film deposited on a templated substrate. The thin film morphology consists of well-ordered in-plane core/shell cylinders in

trenches (t_{trench} ~ 47 nm), oriented along the groove direction while hexagonal out-of-plane nanoring arrays are produced on mesas (t_{mesa} ~ 29 nm). The 2D-FFT exhibits, in addition to the characteristic first-order and higher-order spots of the template and the in-plane core/shell cylinders, six sharp first-order and higher-order spots which is the signature of highly-ordered hexagonal arrays with a single orientation on mesas. The high-resolution contrast of the associated AFM phase image evidenced the formation of out-of-plane nanoscale rings on mesas from which mean inner and outer diameters of ~ 11.2 ± 1.4 nm and ~ 32.2 ± 2.6 nm, respectively, have been measured (see **Fig. S3** and **1b**). Importantly, these results indicate that quite narrow domain size distributions are obtained from templated DSM thin films although higher PS domains are clearly overestimated from AFM images, making the apparent composition deviates from the expected symmetric one (D:S:M = 32:36:32). To demonstrate the formation of highly-ordered nanoring arrays over several micrometers, a lower magnification (4 x 4 μm) AFM image has been taken from the same sample (see **Fig. S4**). Well-ordered in-plane core/shell cylinders oriented along the groove could be observed while a single orientation of hexagonal nanoring arrays is clearly evidenced by the 2D-FFT. For comparison, at a such magnification, the 2D-FFT of a solvent-annealed (3h, $CHCl_3$) 27 nm thick DSM film deposited on flat substrate mainly consists of two isotropic rings indicating that out-of-plane nanorings are ordered within randomly oriented smaller grains (see **Fig. S5**).

The effect of the film thickness on the domain orientation was also studied from templated DSM thin films. Well-ordered out-of-plane nanorings confined in trenches (t_{trench} ~ 31 nm) were produced when the polymer layer is not thick enough to generate a continuous film after the solvent-annealing process (see **Fig. 4a**). Increasing the polymer layer thickness induces the formation of a continuous film where in-plane and out-of-plane core/shell cylinders are formed in trenches (t_{trench} ~ 47 nm) and on mesas (t_{mesa} ~ 29 nm), respectively (see **Fig. 4b** and **S6**). Finally, core/shell cylinders with an in-plane orientation are observed both in trenches (t_{trench} ~

65 nm) and on mesas (t_{mesa} ~ 47 nm) when the film thickness is increased again (see **Fig. 4c** and **S7**). These results indicate the domain orientation could be controlled through the film thickness without using a brush layer to tune the substrate surface energy. A similar domain orientation behavior was recently observed from templated PDMSB-*b*-PMMA (DM) BCP thin films. Indeed, PMMA cylinders with an out-of-plane orientation were produced from a 30 nm DM thick film while an in-plane orientation was demonstrated from a thicker DM layer (t ~ 40 nm).[33]

In order to decrease the periodicity of the nanoring array and improve its long-range order, DSM thin films were blended with small PDMSB-*b*-PS (DS) diblock chains which enable relaxation of longer terpolymer chains, as seen for other linear and star triblock terpolymer systems blended with homopolymers.[34, 35] The addition of DS chains inside the DSM thin film induced several behavior changes within the nanostructure since a decrease of the periodicity and an improvement of the nanoring array ordering is achieved concurrently with the persistence of the out-of-plane domain orientation over a bilayer thick film ($t > 2p$). For instance, blending the DSM thin film with 25 wt. % of DS chains improved the ordering within the nanoring array as revealed by GISAXS data (see **Fig. S8**). Indeed, the broad scattered signal observed for the neat DSM thin film (t ~ 70 nm) is replaced by a sharper Bragg rod scattering on the GISAXS pattern of the blended layer which indicates an improvement of the long-range order within the out-of-plane core/shell cylinder structure. This result is also confirmed by the formation of larger grains (size > 1.5 μm^2) as the one shown on AFM images presented on **Figure 5** produced from a solvent-annealed (3h, $CHCl_3$) 70 nm thick DSM/DS film. The 2D-FFT consisting of six sharp first-order and higher-order spots indicates that the periodicity of the highly-ordered hexagonal array is ~ 33 nm which is 15% smaller than the one observed within neat DSM thin films. This result is also fully-supported by a shift of the Bragg rod position toward higher q-values (see **Fig. S8**). Importantly, solvent-annealed (3h, THF) DS thin

films self-assemble into in-plane cylinders with a small periodicity (p_{cyl} ~ 21.1 nm) (see **Fig. S9**). Therefore, the resulted periodicity, p_{blend}, of the nanoring array obtained from the miscible binary mixture (at the molecular level) of short and long chains satisfies: 21.1 nm < p_{blend} < 38 nm, as demonstrated previously by Hashimoto and coworkers for binary mixtures of diblock copolymers.[36] As previously mentioned, the production of templated thin films consisting of well-ordered out-of-plane nanorings both in trenches and on mesas are highly-desired for some technological applications. To accomplish this point, the blending methodology revealed to be useful as illustrated on **Figure S10** from which core/shell cylinders with an out-of-plane orientation are demonstrated both in trenches (t_{trench} ~ 85 nm) and on mesas (t_{mesa} ~ 55 nm).

In summary, a non-frustrated linear PDMSB-*b*-PS-*b*-PMMA triblock terpolymer was used in this work to successfully fabricate nanoscale ring arrays with a period of 38 nm. Long range ordering of features having mean inner and outer diameters of ~ 11 nm and ~ 32 nm was achieved by directing the self-assembly of PDMSB-*b*-PS-*b*-PMMA with topographical substrates. As the core/shell cylinder orientation is controlled through the polymer layer thickness, highly-ordered out-of-plane nanorings confined in trenches were produced when the polymer layer is not enough thick to generate a continuous film after the solvent vapor annealing process. Out-of-plane orientation of nanoscale rings was also demonstrated both in trenches and on mesas of templates by using a blending methodology. This configuration turns out to be of high interest for a variety of nanotechnological applications such as high density magnetic recording where perfectly-ordered magnetic nanorings with controllable dimension are highly desired.

Experimental Section

Neat and blend DSM thin film preparation: Thin films of neat DSM or blended DSM with DS were spin-coated on templated and smooth silicon substrates using a 1 wt.% polymer

solution in a mixture THF/PGMEA (2/1). The self-assembly of terpolymer thin films was promoted by exposing samples to a continuous stream of $CHCl_3$ vapor. Templated and untemplated film thicknesses have been determined from scratched polymer area and using a Filmetrics F20-UV instrument, respectively.

Topographical grating fabrication: The periodic topographical gratings were fabricated using a Lloyd's mirror interferometer with a 325 nm He-Cd laser beam. To transfer the interference lithography pattern into the Si/45 nm SiO_2 layer, a trilayer resist stack methodology was used. This trilayer was obtained by inserting a hard mask layer consisting of a SiO_2 thick film between a chemically-amplified negative resist resin and an anti-reflection coating (ARC) layer. After development of the resist, the pattern was transferred into the hard mask then into the ARC and finally into the SiO_2 by a series of RIE steps to form a grating.

ALD exposure: Sequential infiltration synthesis (SIS) was performed using an atomic layer deposition (ALD, Ultratech SAVANNAH G2) tool in exposure mode. This mode allowed Al_2O_3 SIS using an alternating exposure of DSM thin films to trimethylaluminum (TMA) and deionized water at 85°C with a purge under N_2 gas flow after each exposition. During exposure time, pressure in ALD chamber increases leading to an infiltration of species in the PMMA domains, then during purge time, unreacted precursor were removed by N_2 flow. Exposure and purge times used in this experiment were 60s and 300s, respectively, for both precursors. In this work, three cycles (TMA/purge/H_2O/purge) of SIS were performed.

AFM Characterization: Atomic force microscopy (AFM Dimension FastScan, Bruker) was used in tapping mode to characterize the surface morphology of terpolymer thin films. Silicon cantilevers (Fastcsan-A) with a typical tip radius of ~ 5 nm were used. The resonance frequency of the cantilevers was about 1.25 kHz. Prior to AFM measurement, DSM thin films were etched with a fluorine-rich RIE treatment using a plasma etch (PE-100, PlasmaEtch) tool

in order to remove preferentially the PDMSB and PMMA phases (plasma conditions are: 40 W, 17 sccm CF_4 and 3 sccm O_2, 180 mTorr, 45 s).

GISAXS Measurement: GISAXS measurements were performed on CRB-BM02 beamline at the European Synchrotron Radiation Facilities (ESRF) in Grenoble using a photon energy of 15 keV. GISAXS patterns were recorded on a XPAD 2D pixel detector (960 × 560 pixels, 130 μm pixel size) placed at a distance of 5000 mm from the sample. To minimize air scattering, the whole path of the scattered beam was under vacuum apart from the nearest region around sample. With the incident beam propagating along the *x* direction, the GISAXS images were recorded in the (q_y, q_z) plane where q_y and q_z are the components of the scattering vector, related to the in-plane angle $2\theta_f$ and out-plane angle α_f. GISAXS patterns were normalized with respect to the incident beam intensity monitored by a front photomultiplier.

Acknowledgements

The authors acknowledge support from Arkema and the Région Nouvelle Aquitaine. D2AM French CRG Beamline is acknowledged for allocating beamtime at ESRF for the GISAXS experiments. The authors would also thank Dr. A. Legrain from LTM who performed GISAXS measurements. This work was performed within the framework of the Equipex ELORPrintTec ANR-10-EQPX-28-01 and the LabEx AMADEUS ANR-10-LABEX-0042-AMADEUS with the help of the French state Initiative d'Excellence IdEx ANR-10-IDEX-003-02 and the LCPO-Arkema INDUSTRIAL CHAIR "HOMERIC" ANR-13-CHIN-0002-01. The research leading to these results has received funding from the ENIAC JU PLACYD project.

REFERENCES

(1) K. Y. Jung, F. L. Teixeira, R. M. Reano, *J. Lightwave Technol.* 2007, **25**, 2757.

(2) Y. Babayan, J. M. McMahon, S. Z. Li, S. K. Gray, G. C. Schatz, T. W. Odom, *ACS Nano* 2009, **3**, 615.

(3) Z. K. Wang, H. S. Lim, H. Y. Liu, S. C. Ng, M. H. Kuok, L. L. Tay, D. J. Lockwood, M. G. Cottam, K. L. Hobbs, P. R. Larson, *et al*., *Phys. Rev. Lett.* 2005, **94**, 137208

(4) A. Kosiorek, W. Kandulski, H. Glaczynska, M. Giersig, *Small* 2005, **1**, 439.

(5) Y. Ren, A. O. Adeyeye, C. Nam, C. A. Ross, *IEEE. Trans. Magn.* 2010, **46**, 1906.

(6) Z. G. Li, P. S. Liu, Y. P. Liu, W. P. Chen, G. P. Wang, *Nanoscale* 2011, **3**, 2743.

(7) A. Lorke, R. J. Luyken, A. O. Govorov, J. P. Kotthaus, J. M. Garcia, P. M. Petroff, *Phys. Rev. Lett.* 2000, **84**, 2223.

(8) J. X. Chen, W. S. Liao, X. Chen, T. L. Yang, S. E. Wark, D. H. Son, J. D. Batteas, P. S. Cremer, *ACS Nano* 2009, **3**, 173.

(9) K. H. Li, Z. T. Ma, H. W. Choi, *Appl. Phys. Lett.* 2011, **98**, 071106.

(10) Q. Pan, R. D. James. *J. Appl. Phys.* 2000, **87**, 4702.

(11) J. Aizpurua, P. Hanarp, D. S. Sutherland, M. Käll, G. W. Bryant, F. J. G. de Abajo, *Phys. Rev. Lett.* 2003, **90**, 057401.

(12) P. Nordlander, *ACS Nano* 2009, **3**, *488.*

(13) Y. Luo, Y. Du, V. Misra, *Nanotechnology* 2008, **19**, 265301.

(14) The core/shell cylindrical morphology for a linear ABC triblock terpolymers was first suggested by Riess *et al*: G. Riess, M. Schlienger, G. Marti, *J. Macromol. Sci., Phys.* 1980, **B17**, 355.

(15) R. A. Segalman, H. Yokoyama, E. J. Kramer, *Adv. Mater.* 2001, **13**, 1152.

(16) S. Park, D. H. Lee, J. Xu, B. Kim, S. W. Hong, U. Jeong, T. Xu, T. P. Russell, *Science* 2009, **323**, 1030.

(17) Y. Rho, K. Aissou, M. Mumtaz, W. Kwon, G. Pécastaings, C. Mocuta, S. Stanecu, E. Cloutet, C. Brochon, G. Fleury, G. Hadziioannou, *Small* 2015, **11**, 6377.

(18) S. Guo, J. Rzayev, T. S. Bailey, A. S. Zalusky, R. Olayo-Valles, M. A. Hillmyer, *Chem. Mater.* 2006, **18**, 1719.

(19) V. P. Chuang, C. A. Ross, P. Bilalis, N. Hadjichristidis, *ACS Nano* 2008, **2**, 2007.

(20) S. Jeon, K. Jang, S. H. Lee, H. Park, B. Sohn, *Langmuir* 2008, **24**, 11137.

(21) V. P. Chuang, C. A. Ross, J. Gwyther, I. Manners, *Adv. Mater.* 2009, **21**, 3789.

(22) M.D. Rodwogin, A. Baruth, E.A. Jackson, C. Leighton, M.A. Hillmyer, *ACS Appl. Mater. Interf.* 2012, **4**, 3550.

(23) H.–J. Jeon, T. Y. Kim, W.–B. Jung, H.–S. Jeong, Y. H. Kim, D. O. Shin, S. J. Jung, J. Shin, S. O. Kim, H.–T. Jung, *Adv. Mater.* 2016, **28**, 8439.

(24) L. Wang, F. Montagne, P. Hoffman, R. Pugin *Chem. Commun.* 2009, **25**, 3798

(25) K. W. Gotrik, A. F. Hannon, J. G. Son, B. Keller, A. Alexander-Katz, C. A. Ross, *ACS Nano* 2012, **6,** 8052.

(26) F. S. Bates MRS Bulletin, 2005, **30**, 525.

(27) T.P. Russell, R.P. Hjelm, P.A. Seeger, *Macromolecules*, 1990, **23**, 890.

(28) K. Aissou, W. Kwon, M. Mumtaz, S. Antoine, M. Maret, G. Portale, G. Fleury, G. Hadziioannou, *ACS Nano* 2016, **10**, 4055.

(29) χ_{DM} was experimentally determined from SAXS profiles acquired in the vicinity of the order-disorder transition (ODT) using theoretical calculations based on the random phase approximation (RPA). The resulting temperature-dependent Flory-Huggins parameter was found to be $\chi_{DM} = 34.16/T + 0.0855$ (with T expressed in K) which is equivalent to a value of 0.2 at 298 K.

(30) M. R. Hammond, S. W. Sides, G. H. Fredrickson, E. J. Kramer, J. Roukolainen, S. F. Hahn, *Macromolecules* 2003, **36**, 8712.

(31) K. Aissou, T. Baron, M. Kogelschatz, A. Pascale, *Macromolecules* 2007, **40**, 5054.

(32) Q. Peng, Y.-C. Tseng, S. B. Darling, J. W. Elam, *Adv. Mater.* 2010, **22**, 5129.

(33) K. Aissou, M. Mumtaz, G. Fleury, G. Portale, C. Navarro, E. Cloutet, C. Brochon, C. A. Ross, G. Hadziioannou, *Adv. Mater.* 2015, **27,** 261.

(34) V. P. Chuang, J. Gwyther, R. A. Mickiewicz, I. Manners, C. A. Ross, *Nano Lett.* 2009, **9**, 4364.

(35) (a) K. Aissou, H. K. Choi, A. Nunns, I. Manners, C. A. Ross, *Nano Lett.* 2013, **13**, 835. (b) K. Aissou, A. Nunns, I. Manners, C. A. Ross, *Small* 2013, **9**, 4077.

(36) F. Court, T. Hashimoto, *Macromolecules* 2002, **35**, 2566.

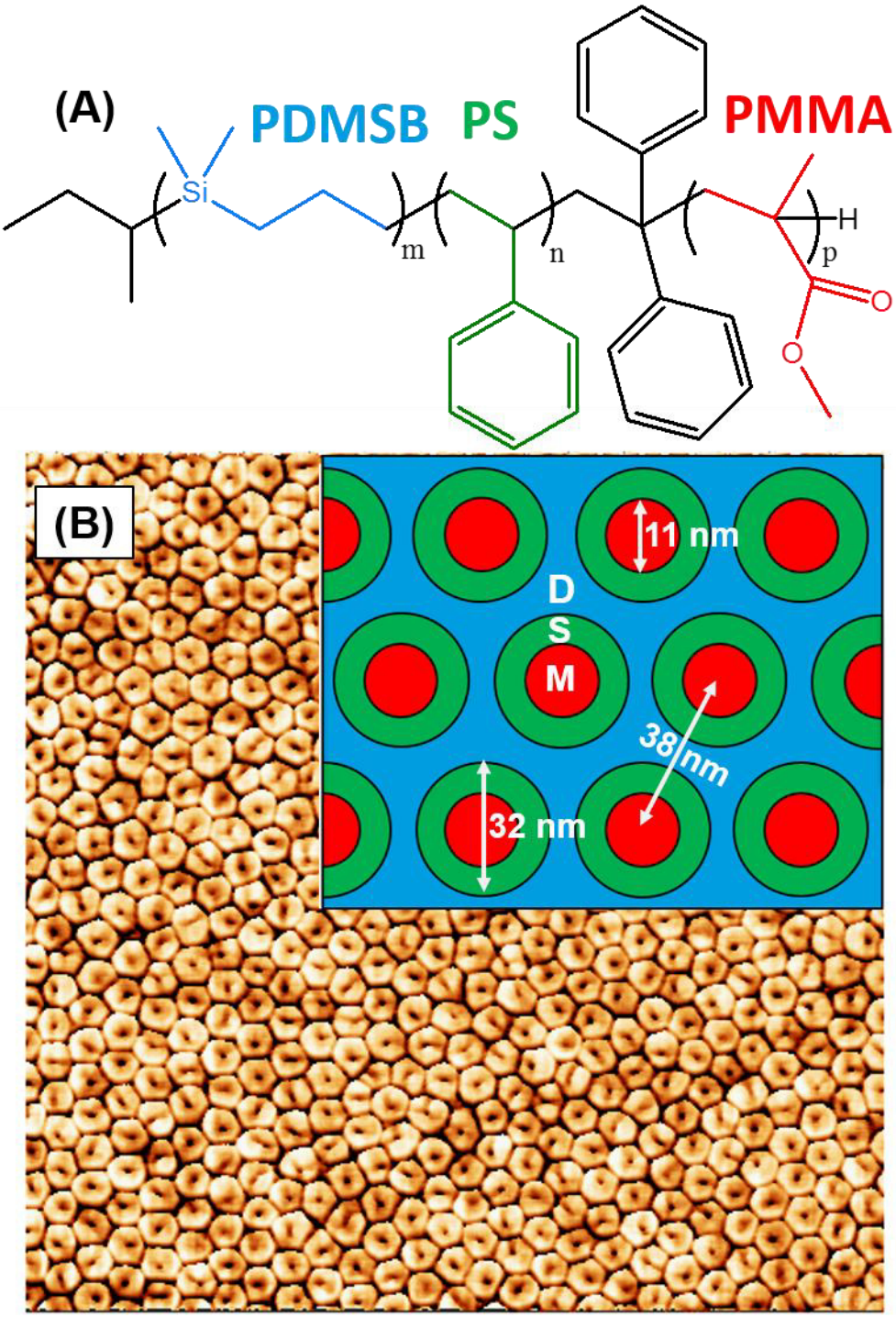

Figure 1. (a) Structure of the linear PDMSB-*b*-PS-*b*-PMMA triblock terpolymer used in this work. (b) (1 x 1 μm) AFM phase view of a solvent-annealed (3h, $CHCl_3$) DSM thin film (t ~ 27 nm) treated by a CF_4/O_2 RIE plasma where bright PS nanorings formed within partially etched PDMSB and PMMA domains are arranged in a hexagonal array of ~ 38 nm period. Inset: Schematic model showing the core/shell microstructure with a *p6mm* symmetry. Scale bar: 200 nm.

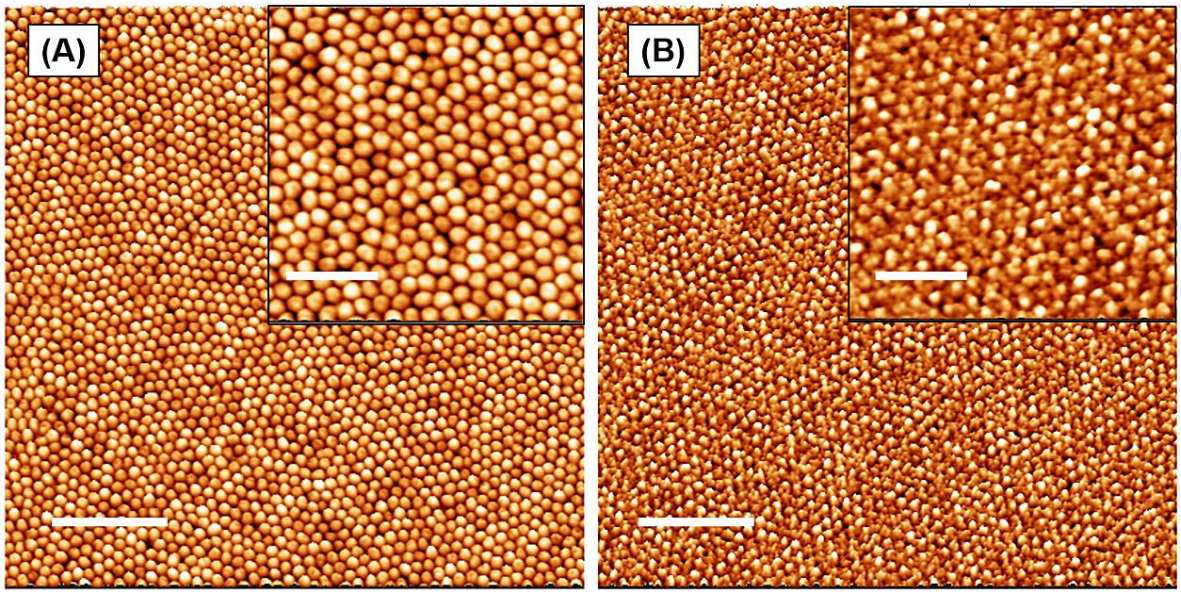

Figure 2. AFM topographic views of a solvent-annealed (3h, $CHCl_3$) DSM thin film (t ~ 27 nm) (a) after a CF_4/O_2 RIE plasma and (b) followed by a Al_2O_3 deposition and UV/O_3 treatment. Insets: magnified AFM topographic images showing an out-of-plane core/shell cylinder structure (a) before and (b) after 3 ALD Al_2O_3 cycles. Scale bars: 200 nm.

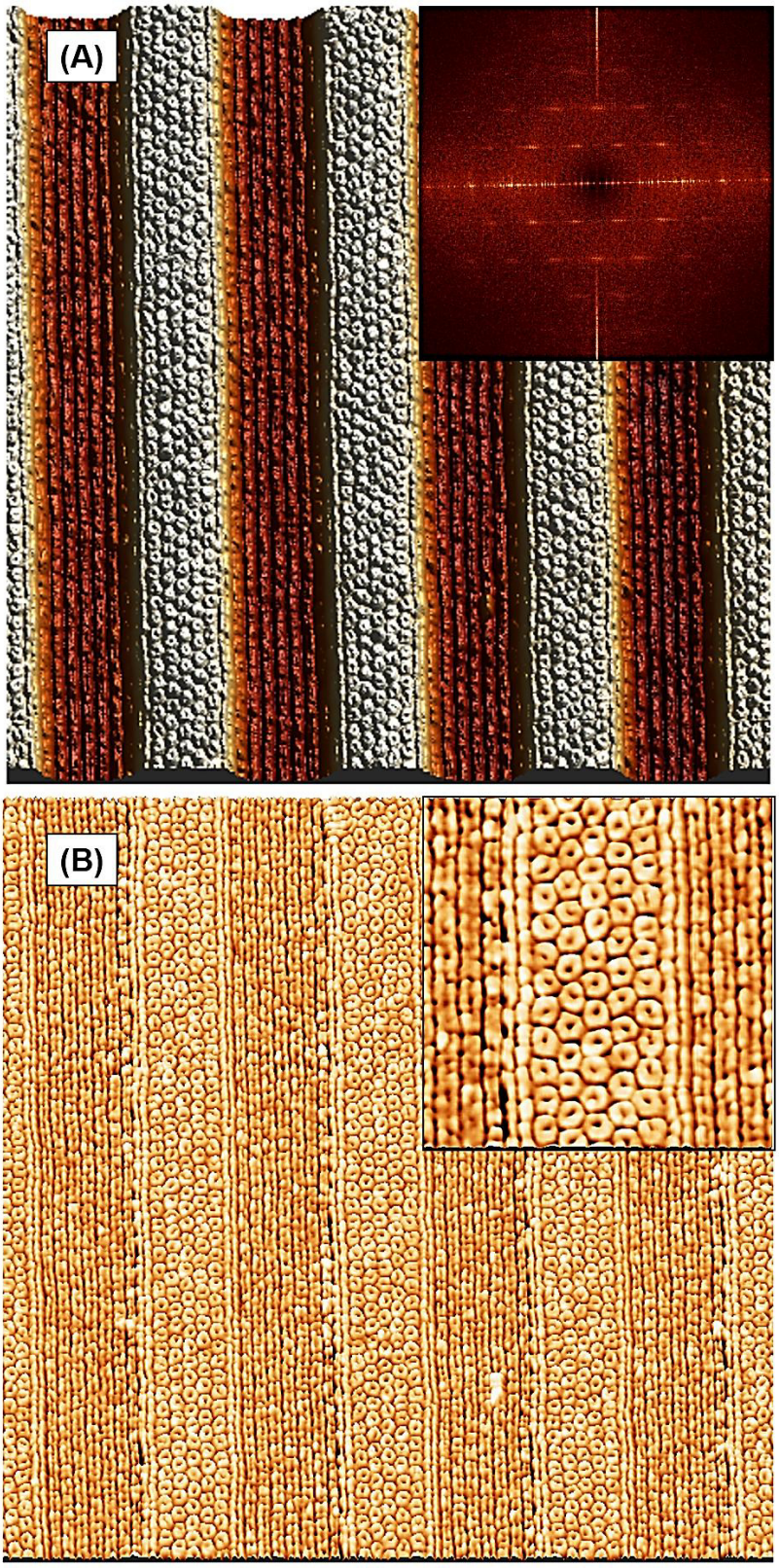

Figure 3. (2 x 2 μm) AFM (a) topographic and its associated (b) phase views of a solvent-annealed (3h, $CHCl_3$) DSM thin film deposited on a topographical substrate and etched by a CF_4/O_2 RIE plasma. Insets: 2D-FFT of the AFM topographic view and a (0.5 x 0.5 μm) AFM phase image showing out-of-plane (bright) PS nanorings on mesas and in-plane core/shell cylinders in trenches.

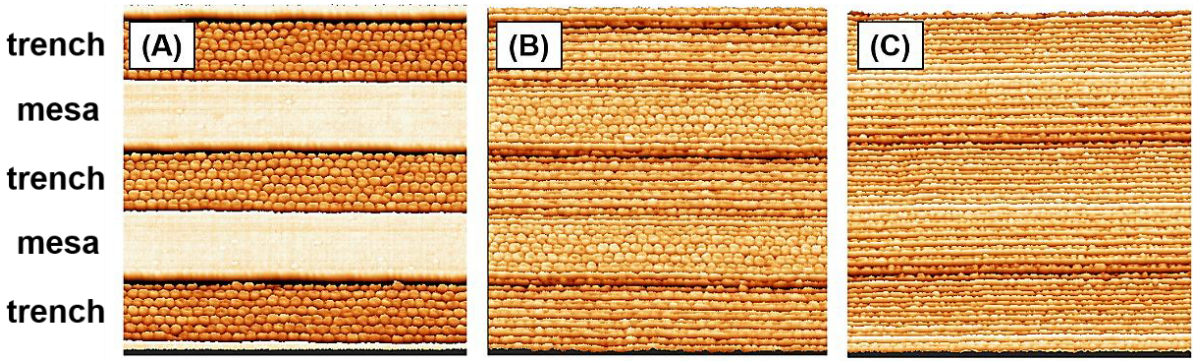

Figure 4. (1.25 x 1.25 μm) AFM phase views of templated DSM thin layers with different film thicknesses: (a) t_{trench} ~ 31 nm, (b) t_{trench} ~ 47 nm and t_{mesa} ~ 29 nm and (c) t_{trench} ~ 65 nm and t_{mesa} ~ 47 nm. DSM thin films were annealed under $CHCl_3$ vapors for 3h then etched by a CF_4/O_2 RIE plasma prior to be imaged by AFM. Positions of trenches and mesas are indicated on the left of the figure.

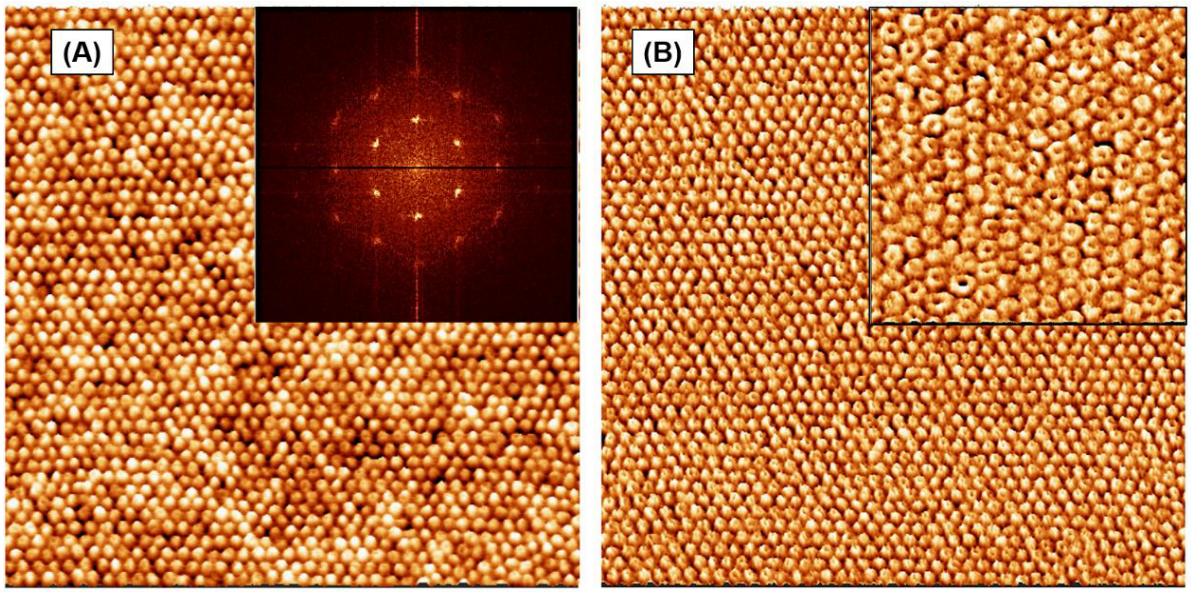

Figure 5. (1.5 x 1.5 μm) AFM (a) topographic and its associated (b) phase views of a solvent-annealed (3h, $CHCl_3$) 70 nm thick DSM layer blended with 25 wt. % of DS chains treated by a CF_4/O_2 RIE plasma. Insets: 2D-FFT of the AFM topographic view and a (0.5 x 0.5 μm) AFM phase image showing out-of-plane (bright) PS nanorings.

Use for TOC only